ADVANCED OPTICAL MATERIALS
www.advopticalmat.de

Hedgehog Inspired CuO Nanowires/Cu_2O Composites for Broadband Visible-Light-Driven Recyclable Surface Enhanced Raman Scattering

Kaichen Xu, Huangping Yan, Chuan Fu Tan, Yuyao Lu, Yang Li, Ghim Wei Ho, Rong Ji, and Minghui Hong**

Self-cleanable surface-enhanced Raman scattering (SERS) spectroscopy affords a promising route toward environment-friendly biosensors for point-of-care diagnostics. It is of great importance to develop recyclable SERS substrates driven by a photocatalytic decomposition process, especially in the visible range. In this work, inspired by the hedgehog-like structures, a broadband visible-light-driven photocatalytic SERS platform with the CuO nanowires (NWs)/Cu_2O hetero-nanostructures as the backbone is demonstrated. Via employing the approach of nanosecond laser ablation on Cu sheet coupled with subsequent thermal oxidation, the formed hedgehog-like, high-density, and dual-scale micro/nanostructures not only demonstrate enhanced broadband visible-light-absorption capability even extended to the near infrared range but also exhibit boosted interfacial adhesion with favorable stability. Such phenomena imply that the binary oxidized Cu composites decorated with metallic nanoparticles can serve as high-performance SERS substrates with superior recyclability. Under the visible light illumination, the as-fabricated ternary Ag/CuO NWs/Cu_2O composites can be self-cleaned by photocatalytic degradation of adsorbates, thus leading to recyclable SERS substrates, which can preserve more than 85% SERS activity after seven cycles' measurement. These results pave a new path to realize reusable SERS substrates in the applications of remote and resource-limited environments toward next-generation green biosensors.

1. Introduction

"Green" materials and nanotechnologies have been envisioned as effective means toward carving a sustainable future.[1] Inspired by this ambitious goal, scientists attempt to develop renewable environment-friendly functional devices to minimize the negative impact on our living surroundings.[2] In particular, reusable biosensors have recently drawn increasing research attention because of their advantages to be applied in remote and resource-limited environments for point-of-care (POC) diagnostics.[3] Among a variety of biosensors, surface-enhanced Raman scattering (SERS) is emerging as one of the most cutting-edge techniques for its intriguing role to demonstrate sensitivity down to the single molecule level.[4–6] Such accurate label-free and fingerprint detection technique has been considered as a promising and noninvasive POC diagnostic tool in various applications, such as environmental monitoring,[7] drug detection,[8] explosives analyses,[9] as well as healthcare inspection.[10] Due to small scattering cross sections of the detected molecules, a plenty of plasmonic nanostructures primarily based on the electromagnetic field enhancement are widely investigated, which usually rely on chemical syntheses or complex lithographic approaches to achieve high-density of hotspots.[11–20] Among them, laser processing is an intriguing approach to fabricate micro/nanostructures over a large area at a high speed.[21–24] Nevertheless, most of these traditional SERS substrates can only be applied as single use due to the cross-contamination of probe molecules.[25,26] The high costs also hinder the practical applications of large-scale production of noble metal-based SERS substrates.

In recent years, recyclable SERS substrates have attracted considerable research attentions because of their self-cleaning characteristics, which typically rely on wide bandgap semiconductors, such as ZnO and TiO_2 as the building block.[27–36] Due to their photocatalytic capability, under the UV light irradiation, the formation of photogenerated oxygen species, such as superoxide radical anions ($O_2^{\bullet-}$) and hydroxyl radicals ($OH^{\bullet}$) result in the decomposition of analytes adsorbed on the

K. Xu, C. F. Tan, Y. Lu, Dr. Y. Li, Prof. G. W. Ho, Prof. M. Hong
Department of Electrical and Computer Engineering
National University of Singapore
4 Engineering Drive 3, Singapore 117576, Singapore
E-mail: elehmh@nus.edu.sg
K. Xu, Dr. R. Ji
Data Storage Institute
(A*STAR) Agency for Science Technology and Research
2 Fusionopolis Way, Singapore 138634, Singapore
E-mail: ji_rong@dsi.a-star.edu.sg
Dr. H. Yan
School of Aerospace Engineering
Xiamen University
422 Siming South Road, Xiamen 361005, P. R. China
Y. Lu
Department of Chemistry
National University of Singapore
3 Science Drive 3, Singapore 117543, Singapore
The ORCID identification number(s) for the author(s) of this article can be found under https://doi.org/10.1002/adom.201701167.

DOI: 10.1002/adom.201701167

SERS substrates.[37–39] With this motivation in mind, a plenty of metal–semiconductor hybrid nanostructures as cleanable SERS substrates have been studied. For instance, Au semi-shells on TiO_2 spheres have been demonstrated via nanosphere self-assembly coupled with subsequent atomic layer deposition (ALD) methods.[29] The UV-assisted cleaning is capable of degrading adsorbates on Au-TiO_2 composite, which can preserve the SERS activity even after five adsorption and UV-cleaning cycles. Furthermore, other emerging self-cleaning SERS substrates have also been reported, including Au-coated ZnO nanorods,[28] TiO_2 nanofibers decorated with Ag nanoparticles,[30] flower-shaped Au-ZnO hybrid composites,[27] as well as ZnO@ZnS-Ag active nanostructures.[40] However, one of the intrinsic drawbacks of the aforementioned reusable SERS substrates is that UV irradiation (only ≈4% of solar spectrum) is required for self-cleaning due to the wide bandgap of ZnO (≈3.37 eV) or TiO_2 (≈3.2 eV), which restricts their practical applications.[37,41] Therefore, it is of great significance to improve the utilization efficiency of solar energy in the visible range for photocatalytic recyclable SERS substrates.

In order to realize the visible-light-driven self-cleanable SERS detection, the backbone material of a hybrid SERS system with the capability to enhance visible light absorption is required to be achieved, although a formidable task. Huang et al. recently demonstrated the chestnut-like Ag/WO_{3-x} nanostructures by a hydrothermal approach and redox reaction for reusable SERS substrates, which can endure multiple visible-light cleaning.[42] Furthermore, the incorporation of gold nanoparticles graphitic carbon nitride into graphene oxide (GNPs/g-C_3N_4/GO) was reported to exhibit both good SERS and catalytic activity for the detection as well as removal of adsorbates illuminated by visible light.[11] However, the majority of conventional reported reusable SERS substrates are provided with narrow light absorption band and furthermore, generally involve several tedious fabrication procedures.[11,33,42] Hence, it is highly expected to develop a recyclable SERS system by a facile fabrication approach, which is capable of being driven by wideband visible light illumination to achieve the target of self-cleaning property.

The rising star of copper oxide-based nanostructures, especially nanowires, is conceived to be an alternative candidate because of their prominent superiority as a p-type semiconductor with a narrow bandgap.[43,44] Stimulated by this excellent property, herein, a new type of ternary hetero-nanostructured Ag/CuO nanowires (NWs)/Cu_2O composite is demonstrated as the broadband visible-light-driven recyclable SERS detection. Via employing the nanosecond laser processing on Cu sheet and subsequent thermal oxidation, the hedgehog-like and dual-scale binary composite of CuO NWs/Cu_2O is formed as the building block, followed by the decoration of Ag nanoparticles to achieve the reusable SERS substrates, which can be self-cleaned under the visible light illumination. This approach represents several advantages. First, different from the conventional vertical-aligned CuO NWs' growth on the flat Cu plate/sheet surface, the strategy of nanosecond laser processing can produce the microgrooves array on the Cu sheet surface, which enables the formation of horizontal and hierarchical nanostructured CuO NWs with enhanced adhesion on the microtextured Cu sheet through thermal oxidation. Second, the improved growth of hierarchical and high-density CuO NWs with high aspect ratios decorated with metallic nanoparticles can boost the light–matter interactions with the excitation photons, which is able to improve the intensity of SERS signals. Third, the CuO NWs/Cu_2O hetero-nanostructures can enhance and extend the visible light absorption even to the near-infrared range primarily due to the narrow bandgap of oxidized Cu composites. Such intriguing feature affords an excellent opportunity to develop broadband visible-light-driven photocatalytic SERS substrates. The ternary Ag/CuO NWs/Cu_2O nanostructures endowed with the facile fabrication strategy, enhanced visible-light response as well as the boosted SERS signals initiate the path toward new environment-friendly biosensors.

2. Results and Discussion

To develop a high-performance recyclable SERS sensor, it is of great importance to generate high density of hotspots within a large detection volume. First, a Cu sheet at a thickness of ≈150 µm is pretreated by a pulsed nanosecond laser, giving rise to the formation of microgrooves array (**Figure 1**). It should be noted that the pattern of microgroove arrays with the period as small as possible is selected in order to increase the effective surface area. Then, thermal oxidation is applied to grow CuO

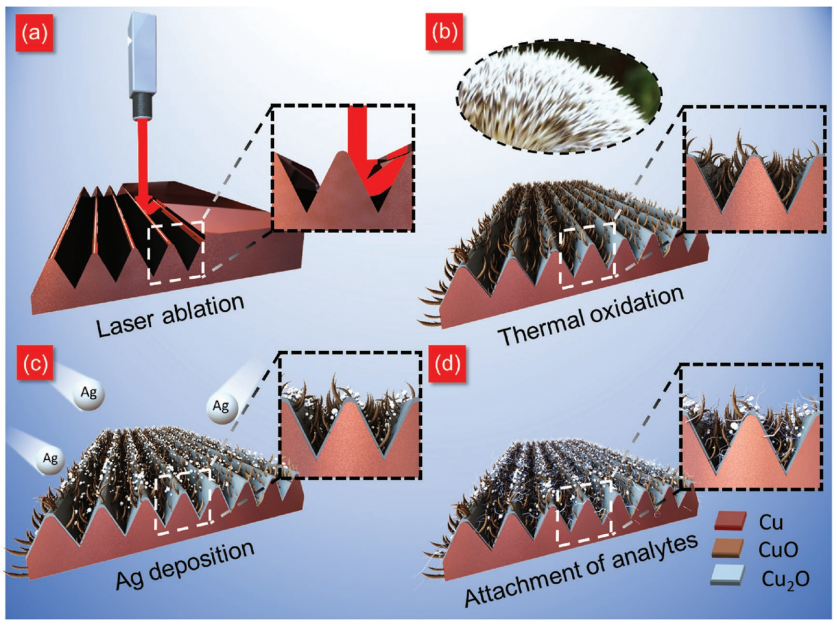

Figure 1. Schematic diagrams of fabricating the ternary Ag/CuO NWs/Cu_2O composite. a) Fabrication of microgrooves array on the Cu sheet. b) Preparation of binary CuO NWs/Cu_2O composite. c) Deposition of Ag nanoparticles onto the binary CuO NWs/Cu_2O composite. d) Attachment of analytes for SERS detection. The inset in (b) shows the optical image of hedgehog's skin.

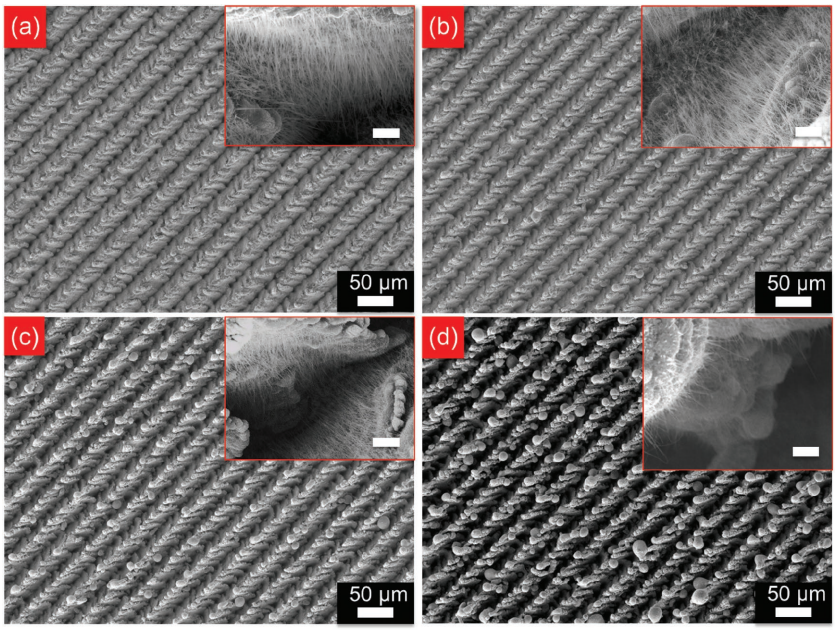

Figure 2. SEM images of hedgehog-like CuO NWs/Cu_2O composite on Cu sheets fabricated by pulsed nanosecond laser processing at different laser fluences and subsequent thermal oxidation. The laser fluence is a) 15, b) 20, c) 25, and d) 30 J cm^{-2}, respectively. The scale bars of the insets are 1 μm. The temperature of thermal oxidation is 450 °C for 2 h. (Laser parameters: pulse duration $\tau = 5$ ns, pulse repetition rate PRR = 90 kHz, laser spot size ≈20 μm, and laser beam scanning speed $\nu = 5$ mm s^{-1}).

NWs on the microtextured Cu sheet to achieve hedgehog-like dual-scale micro/nanostructures. Although tremendous efforts have been devoted to exploring various methods to synthesize CuO NWs, including the electrochemical approach,[45] solution-based routes,[46] and template-based techniques,[47] thermal oxidation is a unique and promising one, which not only affords a rapid, facile, and effective route but also produces much higher quality of CuO NWs with larger aspect ratios.[48,49] Finally, Ag nanoparticles are deposited by an electron-beam evaporator to make the reusable SERS substrates active.

First of all, it is essential to reveal the surface morphology of the hybrid dual-scale micro/nanostructures via the laser ablation and subsequent thermal oxidation. **Figure 2** shows the influence of laser fluence on the surface morphology of microgrooves as well as the distribution and density of CuO NWs. When the intensity of laser fluence is beyond the vaporization threshold of Cu, melting and vaporization occur on the Cu surface, which results in the formation of V-shaped microgrooves along the uniaxial laser scanning on the Cu sheet surface. After the thermal oxidation, there are high-density, high-aspect-ratio, and hierarchical CuO NWs formed on the sidewall skins of microgrooves (Figure 2a–c). The high-resolution cross-section image exhibits that the CuO NWs are uniformly distributed within the microgrooves (Figure S1, Supporting Information). For comparison, the CuO NWs' growth on the Cu sheet without pretreatment by laser is also investigated, which shows the sparser morphology of CuO NWs (Figures S2 and S3, Supporting Information). Meanwhile, it is found that the laser-treated Cu sheet coupled with subsequent thermal oxidation can enhance the interfacial adhesion between the oxide layer and beneath Cu sheet (Figure S4, Supporting Information). The introduction of microgrooves array in advance enables the thermal stress induced by thermal oxidation to be released into the free space, which is capable of inhibiting the oxide layers from cracking or exfoliation.[44,45] It should be noted that if the laser fluence is too high, higher compressive forces are produced by the vapor and plasma plume, which leads to the expulsion of molten pool materials from the laser irradiation area. The higher intensity of laser fluence can extend the heat affected zone, where more molten materials are generated. These molten materials are pressed out of the ablation zone and then solidified, which gives rise to the deeper microgrooves and larger size of microparticles re-deposited onto the surface (Figure 2d). Such regenerated microparticles inhibit the growth of CuO NWs on them. This phenomenon is due to that as the growth of CuO NWs during thermal oxidation is widely considered to follow the mechanism of stress-induced grain-boundary diffusion, the formation of porous Cu_2O and CuO grain layers served as the precursors plays a critical role, where Cu cations can be driven outward.[44,50] However, the microparticles induced by higher laser fluence enable the formation of complex dense oxidized Cu composites, which inhibit the continuous diffusion of Cu ions, resulting in the production of spare CuO NWs after thermal oxidation (Figure S6, Supporting Information).

The crystallographic structures of the as-prepared products are investigated by X-ray diffraction (XRD) analyses (**Figure 3**a). In all patterns, there is a relatively weak diffraction peak at 43.3° and a strong diffraction peak at 50.4°, which comes from the Cu sheet substrate (JCPDS 04-0836). After the laser treatment, the Cu_2O is first formed at smaller laser fluence, where the diffraction peaks at 36.5° and 42.4° indexed to cubic Cu_2O (JCPDS 65-3288) can be clearly distinguished. As the laser fluence is increased, the relative intensity of the peak corresponding to Cu_2O becomes stronger. Meanwhile, new diffraction peaks at 35.6°, 38.8°, and 48.7° representing the monoclinic CuO pattern (JCPDS 1-1117) can be observed. After the thermal oxidation, the peaks representing CuO phases can be seen in all the samples, including the product without laser processing. To further confirm the chemical states of Cu in the oxidized composites, X-ray photoelectron spectroscopy (XPS) measurements are performed (Figure 3b). Four peaks are observed from Cu $2p_{3/2}$ signals. The peak at 932.7 eV corresponds to Cu^{1+}, indicating the generation of Cu_2O. The other peak at 934.7 eV and two more satellite peaks at 941.3 and 943.5 eV represent the oxidation states of Cu^{2+}, confirming the existence of CuO. Meanwhile, the optical features of the CuO NWs/Cu_2O composites are studied by a UV–vis spectrometer (Figure 3c). It is found that the CuO NWs/Cu_2O hetero-nanostructures demonstrate a good performance on visible light absorption due to the narrow bandgap of oxidized Cu composites. Particularly,

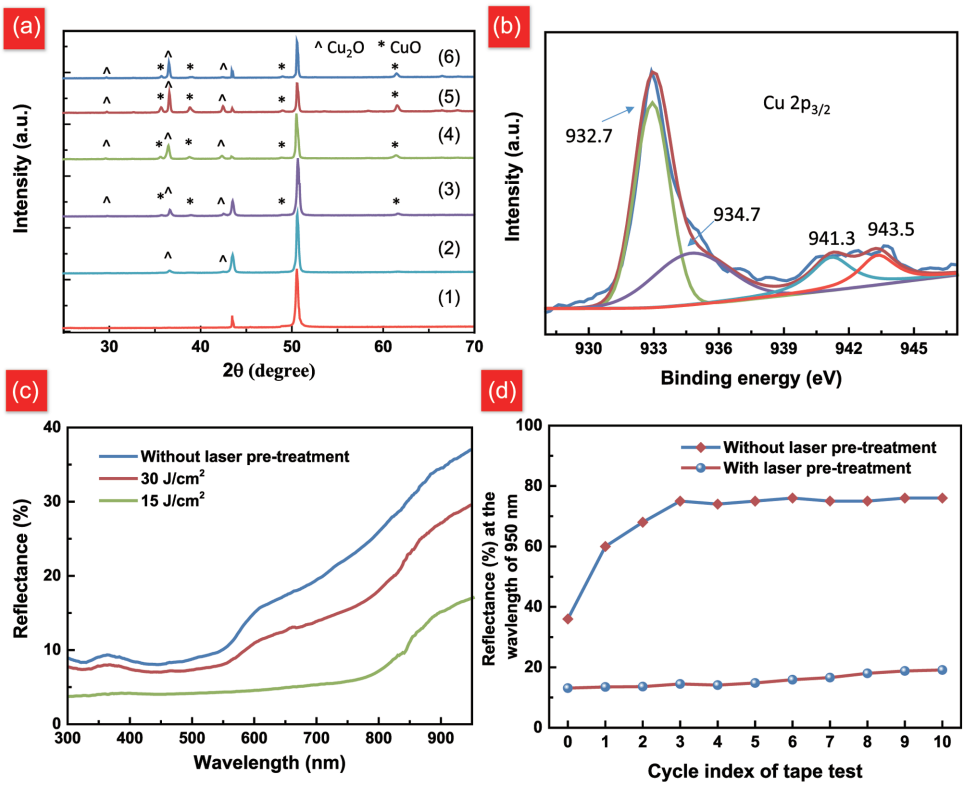

Figure 3. a) XRD patterns of (1) Cu sheet, (2) Cu sheet treated at a laser fluence of 15 J cm^{-2}, (3) Cu sheet treated at laser fluence of 30 J cm^{-2}, (4) and (5) Cu sheet with laser treatment (15 and 30 J cm^{-2}) and subsequent thermal oxidation, and (6) Cu sheet after thermal oxidation. b) XPS spectra of Cu $2p_{3/2}$ for the product with the laser pretreatment and subsequent thermal oxidation. c) Reflectance spectra of the Cu sheets treated at different laser fluences and subsequent thermal oxidation. d) Reflectance intensity at the wavelength of 950 nm for oxidized Cu sheet with and without laser pretreatment after ten cycles' tape test. The period is 30 µm for the sample with laser pretreatment. The temperature of thermal oxidation is 450 °C for 2 h. (Laser parameters: $\tau = 5$ ns, PRR = 90 kHz, laser spot size ≈20 µm, and $\nu = 5$ mm s^{-1}).

the CuO NWs grown from the laser-treated Cu sheet at the laser fluence of 15 J cm^{-2} exhibit a superior antireflection property, which extends the light absorption edge even to the near-infrared range (≈900 nm). Such high-absorption feature further indicates that high-density and hierarchical CuO NWs are formed after the laser treatment and subsequent thermal oxidation of the Cu sheets, which implies that CuO NWs are expected to be excellent backbones for broadband visible-light-driven photocatalysts to achieve recyclable SERS detection. For the products textured at much higher laser fluence (30 J cm^{-2}), the reflective intensity becomes higher because of less density of CuO NWs formed. Furthermore, the adhesion between CuO NWs/Cu_2O composites and Cu sheet is of paramount importance, especially in the reusable SERS detection. It is observed from Figure 3d that the oxidized Cu sheet with laser pretreatment demonstrates high stability of reflectance intensity at the wavelength of 950 nm after ten cycles' tape test, indicating the hybrid CuO NWs/Cu_2O nanostructures can be well stabilized on the Cu sheet without exfoliation, which is the prerequisite for recyclable SERS applications. However, the reflectance intensity at 950 nm for the flat Cu sheet after sole thermal oxidation increases dramatically due to the exfoliation of oxidized Cu composites.

The fabricated hedgehog-like, high-density, and dual-scale CuO NWs/Cu_2O hetero-nanostructures with large surface areas can be employed as an effective platform for a variety of applications. For instance, after decorating the Ag nanoparticles, the CuO NWs/Ag composites are able to offer high density of plasmonic hotspots, which can be employed as the active SERS substrates. First, it is essential to reveal the SERS performance of Cu-based substrates without laser pretreatment. **Figure 4**a demonstrates the SERS spectra of 4-methylbenzenethiol (4-MBT) molecules adsorbed on Ag deposited CuO NWs and flat Cu sheet surface in comparison to those without Ag decoration. As can be seen, there are no peaks observed for the platforms of both flat Cu sheet as well as the Cu sheet with NWs. After depositing a layer of Ag film at a thickness of 15 nm, a significant enhancement at the 1580 cm^{-1} Raman band can be seen. Particularly, compared with the Ag film deposited on flat Cu sheet surface, the CuO NWs decorated with Ag film exhibit around five times higher enhancement due to the higher density of CuO NWs providing the larger surface area to be attached with Ag nanoparticles, which can serve as hotspots for enhancing Raman signals. It should be noted that 15 nm Ag film can form nanoparticles on CuO NWs, while the thicker Ag film (45 nm) can only result in continuous film structures, which are not beneficial for improving SERS signals (Figure 4b). In order to demonstrate the superiority of pulsed laser processed Cu sheet for growing CuO NWs on SERS activity, Figure 4c compares the SERS performance of

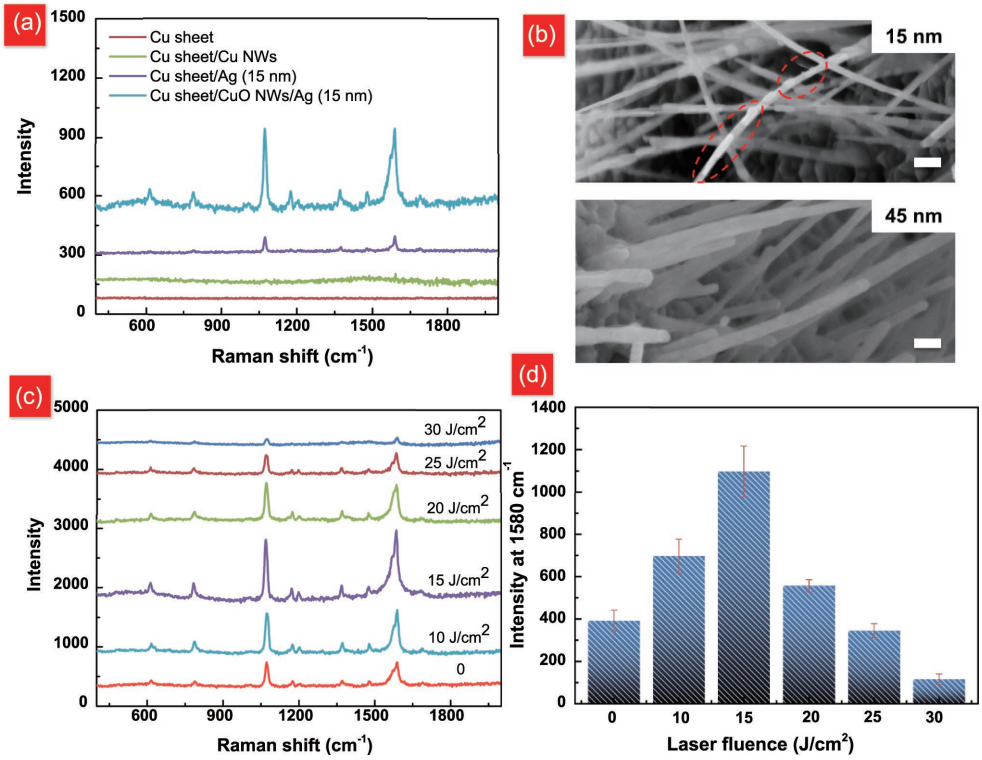

Figure 4. a) SERS spectra of 4-MBT molecules adsorbed on different substrates (without laser processing). b) SEM images of Ag films at the thickness of 15 and 45 nm deposited onto the CuO NWs. The scale bars are 100 nm. c) Influence of laser fluence on SERS performance. d) Average SERS intensity at 1580 cm^{-1} Raman band at different laser fluences. The error bar lines denote the standard deviation from five measurements. The temperature of thermal oxidation is 450 °C for 2 h. All the SERS spectra are obtained at the laser excitation wavelength of 514 nm, power 0.15 mW, acquisition time 10 s, and accumulation time 1. (Laser parameters: $\tau = 5$ ns, PRR = 90 kHz, laser spot size ≈20 µm, and $v = 5$ mm s^{-1}).

the hybrid Ag and oxide Cu-based composites at different laser fluences, while Figure 4d depicts the corresponding change of average SERS intensity at the 1580 cm^{-1} Raman band. It is found that when the laser fluence reaches 15 J cm^{-2}, the SERS signals demonstrate the maximum enhancement, which is around 300% higher than that of Ag nanoparticles deposited onto the thermal-oxidized Cu sheet surface without laser pretreatment. However, the SERS signals become lower by increasing the laser fluence. When the laser fluence is up to 30 J cm^{-2}, the SERS signals are very weak (only ≈70 counts) for 1580 cm^{-1} peak. This phenomenon is because the higher laser fluence results in the deeper depth (tens of µm) of microgrooves, which enables the SERS signals being confined inside the higher microgrooves and can hardly be collected. Furthermore, the microgrooves induced by the higher laser fluence can only grow very lower-density CuO NWs, providing limited surface areas to be attached with Ag nanoparticles and then the fewer hotspots to enhance SERS signals.

In practical applications, it is highly crucial to realize renewable SERS substrates, which can be self-cleaned for reproducible SERS detection. To achieve such a promising goal, it is first essential to evaluate the photocatalytic performance of the as-fabricated ternary Ag/CuO NWs/Cu_2O composites. **Figure 5**a demonstrates the absorption spectra of malachite green (MG) analytes degraded by the ternary Cu oxide-based composites at different time intervals driven by visible light irradiation. Due to its potential risks on human health including carcinogenic probabilities and organ damages, MG has been restricted in use among aquaculture and industries. It is observed that the absorption intensity of MG decreases apparently, indicating the decomposition of MG by the ternary Ag/CuO NWs/Cu_2O heterojunctions. The time-dependent concentration of MG relative to its initial concentration (C/C_0) catalyzed by different composites is plotted in Figure 5b. Obviously, the degradation efficiency of Ag/CuO NWs/Cu_2O composite is much faster than others. Such prominent photocatalytic performance of the ternary catalyst can be primarily attributed to the narrow bandgaps of Cu_2O (2.2 eV) and CuO (1.7 eV) composites, both of which are capable of enhancing the absorption of broadband visible light, leading to the production of electron–hole pairs (Figure 5c). The photogenerated electrons are then transferred from Cu_2O to the conduction band (CB) of CuO. Simultaneously, the holes' transfer occurs in the reverse direction.[37,43] Meanwhile, a portion of photoexcited electrons is moved from CB of CuO to Ag, improving the separation efficiency of charge carriers.[37] The photoinduced electrons and holes allow the formation of superoxide radical anions ($O_2^{\bullet-}$) and hydroxyl radicals ($OH^{\bullet}$), respectively, which can principally decompose organic species into CO_2 and H_2O.[37] Furthermore, the large surface areas of CuO NWs as well as the hedgehog-like and dual-scale micro/nanostructures boost light–matter interactions. The synergistic effect of these factors contributes to the improved decomposition efficiency of MG molecules by the ternary Ag/CuO NWs/Cu_2O composite under the irradiation

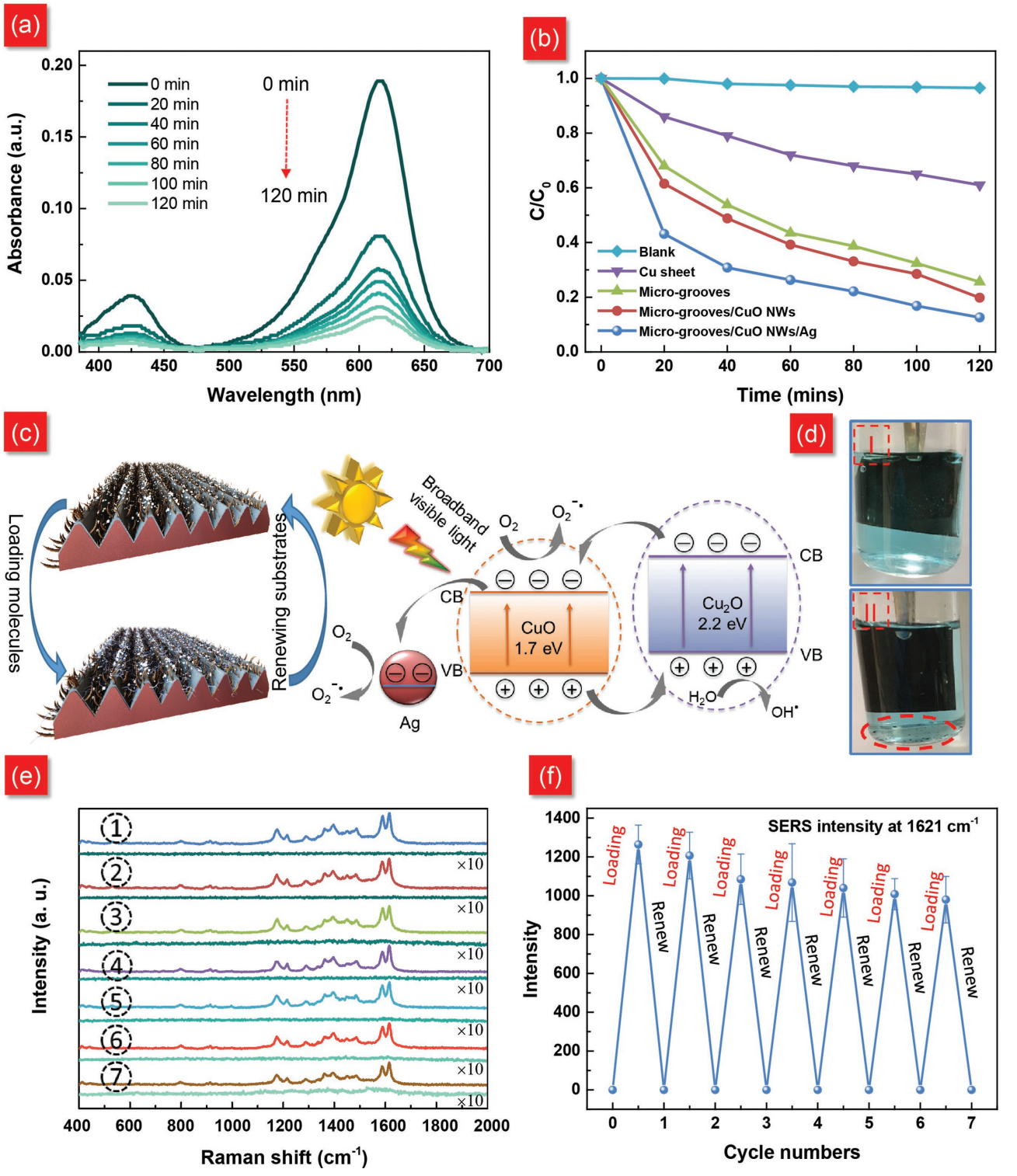

Figure 5. a) UV–vis absorption spectra of MG solution degraded by the ternary Ag/CuO NWs/Cu_2O composites. b) Time-dependent photodegradation efficiency of MG without photocatalysts and in the presence of Cu sheet, Cu sheet after laser ablation, Cu sheet with laser ablation, and subsequent thermal oxidation and Cu sheet with laser ablation and subsequent thermal oxidation decorated with Ag nanoparticles. c) Schematic illustration of broadband visible-light-driven recyclable SERS and mechanisms of the photodegradation. d) Optical images of oxidized Cu sheet with (I) and without (II) laser pretreatment in the photodegradation after 10 min. The dashed circle line denotes the debris exfoliated from the oxidized Cu sheet. e) SERS spectra of MG before and after self-cleaning measurement and f) corresponding average Raman intensities at 1621 cm^{-1} after seven times' recycling test.

of visible light. Notably, the Cu sheet after the laser ablation demonstrates good photodegradation performance because of the formed Cu oxide-based compounds, which can be verified by the aforementioned XRD patterns. It should be noted that Cu sheet also exhibits slight photocatalytic activity due to a thin oxide layer on the pristine Cu sheet.[51] Significantly, the black debris is observed in the reaction container degraded by the ternary composite after 10 min without laser pretreatment due to the exfoliation of oxide composites, while the other one exhibits purer solution with laser pretreated composites because of the enhanced interfacial adhesion (Figure 5d). Such phenomenon implies that the Cu sheet pretreated by the laser and subsequent thermal oxidation can endure multiple cycles of photodegradation and the SERS performance is expected to be preserved. Therefore, the as-fabricated ternary Ag/CuO NWs/Cu_2O composite not only demonstrates superior SERS detection capability but also exhibits excellent photocatalytic activity as well as intensive interfacial adhesion. These three features are expected to be coupled to construct the recyclable and durable SERS systems.

Figure 5e depicts the SERS spectra of MG adsorbed onto the ternary Cu oxide-based composite before and after visible light irradiation. It can be observed that the Raman peaks of MG molecules can be clearly distinguished before the visible light irradiation. When the SERS substrate is illuminated under the visible light, the SERS signals of MG almost disappear because of the photodegradation of adsorbed analytes. Furthermore, the reattachment of molecules is able to recover the similar SERS spectrum. Finally, after seven cycles' measurement, the as-fabricated SERS substrates can still preserve high SERS activity (more than 85%), which is acceptable to satisfy the requirement of recyclable SERS detection (Figure 5f). The slight degradation of SERS performance is probably due to the dissolution of partial Ag nanoparticles in the solution, leading to the reduction of hotspots. These results indicate that our as-fabricated reusable SERS substrates driven by the broadband visible light are expected to serve as environment-friendly biosensors to be applied in remote and resource-limited settings.

Although multiple reusable SERS substrates have attracted great research attentions in recent years due to their self-cleanable characteristics based on strategies of thermal annealing,[52,53] UV-light cleaning,[11,29,30,36] or ethanol-assisted desorption,[54] the broadband visible-light-driven recyclable SERS detection still remains a virgin land. Our work employs the hedgehog-inspired and narrow bandgap of Cu oxide-based nanostructures as the backbone. Different from traditional CuO NWs grown from flat Cu substrates, this work applies nanosecond pulsed laser processing for texturing Cu sheet, allowing the formation of microgrooves array. The oxidized Cu composites not only demonstrate enhanced and extended visible light absorption but also show intensive interfacial adhesion. These superior and distinct features afford remarkable opportunities to achieve reusable SERS substrates driven by the broadband visible light. Furthermore, the designed performance-enhanced thermal-oxidized Cu sheet can be extended toward a variety of promising applications, such as field emission,[55] gas sensing,[56] energy storage,[57] as well as pyroelectricity generation.[58]

3. Conclusions

In conclusion, we have successfully realized broadband visible-light-driven recyclable SERS substrates through CuO NWs/Cu_2O hetero-nanostructures as the building block. Via employing the nanosecond laser ablation and subsequent thermal oxidation on the Cu sheet, the hedgehog-like and higher density of CuO NWs are created on the skin of laser-induced microgrooves array. The as-fabricated CuO NWs not only exhibit the enhanced adhesion on the in situ substrate but also demonstrate the boosted absorption of visible light even extended to the near-infrared range, which affords an excellent backbone for self-cleanable SERS substrates. After the decoration of Ag nanoparticles, the hedgehog-like SERS substrates demonstrate more than 15 times higher enhancement in comparison with that of Ag nanoparticles deposited onto the flat Cu sheet, which is primarily attributed to the higher density of CuO NWs with larger aspect ratios. Furthermore, the as-prepared SERS substrates composed of ternary Ag/CuO NWs/Cu_2O can be self-cleaned through the photodegradation process to decompose analytes under the visible light illumination, leading to the realization of recyclable SERS substrates. Our multiple reusable SERS substrates with distinct features of broadband visible-light-driven capability as well as the facile fabrication strategy are conceivable to be applied in the remote and resource-limited environments for next-generation POC diagnostics.

4. Experimental Section

Preparation of Ag/CuO NWs/Cu_2O Composite: The copper sheet with a thickness of ≈150 µm was cut into pieces of around 2 cm × 2 cm and cleaned with distilled water, followed by nitrogen drying. A nanosecond pulsed laser ablation system was applied to create microgrooves array on the Cu sheet in ambient air. The laser wavelength is 1064 nm with the pulse duration (τ) of 5 ns, pulse repetition rate (PRR) of 90 kHz, laser spot size of ≈20 µm, and laser scanning speed of 5 mm s^{-1}. A hotplate was then employed to heat the corresponding copper sheets in ambience. The temperature of the hotplate can be tuned to arbitrary temperatures. An IR camera was used to monitor the surface temperature of the hotplate. The Cu sheet after the laser processing was then heated on the hotplate to allow the growth of CuO NWs/Cu_2O composite. For comparison, Cu sheet without laser irradiation was also heated to fabricate oxide Cu composites. Finally, Ag nanoparticles were deposited by a BOC Edwards AUTO 306 electron-beam evaporator on the as-fabricated binary CuO NWs/Cu_2O for SERS detection. The vacuum was pumped down to 4.0–5.0 × 10^{-6} Pa with the deposition rate at 0.06 nm s^{-1}. A quartz crystal oscillator was applied to monitor the film thickness.

Characterization: Field emission scanning electron microscope (FESEM, JEOL FEG JSM 7001F) was applied to untangle the morphologies of Cu sheet surface irradiated by the laser, as well as the distribution of Cu NWs. The hybrid nanostructures were investigated by XRD (X' Pert PRO MRD) with Cu Kα radiation at a voltage of 40 kV and current of 40 mA. The scan range is from 10° to 30° at a step size of 0.02° and time per step of 10 s. A CRAIC UV–vis–NIR microspectrometer QDI 2010 was employed to obtain absorbance spectra of the hybrid nanostructures from 300 to 950 nm. To evaluate the adhesion of laser-assisted growth of CuO NWs on the Cu sheet, a scotch adhesive tape was attached onto the sample surface and then peeled off slowly.

SERS Capability Characterization: To evaluate the SERS performance of the heterostructured Ag/CuO NWs/Cu_2O composites, the

nanostructures were functionalized with a self-assembled monolayer of 4-MBT. The SERS-active substrates were submerged inside a 10×10^{-3} M 4-MBT solution made with ethanol for 8 h to allow the formation of self-assembled monolayer and then rinsed in an ethanol solution for 30 s, followed by nitrogen drying.[59] A Renishaw 2000 Raman imaging microscope equipped with a 514 nm continuous wave (CW) laser was used for all experimental characterization. The Raman signals were collected through a 50× (NA = 0.8) microscope lens and detected by a thermoelectrically cooled CCD array. The intensity of laser power is ≈0.15 mW with acquisition time of 10 s and accumulation time of 1. The spectral resolution is 1 cm^{-1}.

Photocatalytic Activity Measurements: The photocatalytic performance of the as-prepared Ag/CuO NWs/Cu_2O composites (effective surface area: 2 cm × 2 cm) was evaluated by degradation of MG, a hazardous dye widely applied in aquaculture. The sample was immersed in MG solution (10^{-5} M, 10 mL) and retained in dark for 30 min to reach the adsorption equilibrium. The above solution with the sample was then irradiated under a xenon lamp equipped with a 400 nm cut-off filter. The UV–vis spectrophotometer was applied to monitor the concentration of MG every 20 min. To make a comparison, the photocatalytic efficiency of the pure Cu sheet, laser-processed Cu sheet, pure Cu sheet after only thermal oxidation, and laser pretreated Cu sheet after subsequent thermal oxidation was also characterized.

Recyclable SERS Characterization Driven by Broadband Visible Light: For recyclability demonstration, the fresh Ag/CuO NWs/Cu_2O composites were first adsorbed with MG molecules (10^{-5} M) for SERS measurements. Then, the above samples were immersed into deionized water on a stir plate and illuminated by the xenon lamp for 1 h. To remove the residual ions and small molecules, the composites were rinsed with deionized water for several rounds and dried by nitrogen. Finally, the substrates were applied to detect MG under the same experimental conditions. Such cycle was repeated for seven rounds for recyclable SERS detection. For the recyclable SERS characterization, the intensity of laser power is ≈1.5 mW with acquisition time of 10 s and accumulation time of 1.

Supporting Information

Supporting Information is available from the Wiley Online Library or from the author.

Acknowledgements

K.X. and H.Y. contributed equally to this work. This research was supported by A*STAR, SERC 2014 Public Sector Research Funding (PSF) Grant (SERC Project No. 1421200080) and Open Project Program of Laser Precision Machining Engineering Technology Research Center of Fujian Province (Grant No. 2016JZA001).

Conflict of Interest

The authors declare no conflict of interest.

Keywords

broadband absorption, CuO nanowires, laser ablation, recyclable surface enhanced Raman scattering, visible-light-driven photocatalysts

Received: November 2, 2017
Revised: January 11, 2018
Published online:

[1] M. Irimia-Vladu, *Chem. Soc. Rev.* **2014**, *43*, 588.
[2] N. Espinosa, A. Laurent, G. A. dos Reis Benatto, M. Hösel, F. C. Krebs, *Adv. Eng. Mater.* **2016**, *18*, 490.
[3] S. Choi, *Biotechnol. Adv.* **2016**, *34*, 321.
[4] J.-F. Li, Y.-J. Zhang, S.-Y. Ding, R. Panneerselvam, Z.-Q. Tian, *Chem. Rev.* **2017**, *117*, 5002.
[5] J. C. Dong, R. Panneerselvam, Y. Lin, X. D. Tian, J. F. Li, *Adv. Opt. Mater.* **2016**, *4*, 1144.
[6] C. Tian, Y. Deng, D. Zhao, J. Fang, *Adv. Opt. Mater.* **2015**, *3*, 404.
[7] K. Xu, Z. Wang, C. F. Tan, N. Kang, L. Chen, L. Ren, E. S. Thian, G. W. Ho, R. Ji, M. Hong, *ACS Appl. Mater. Interfaces* **2017**, *9*, 26341.
[8] D. Li, L. Tang, J. Wang, X. Liu, Y. Ying, *Adv. Opt. Mater.* **2016**, *4*, 1475.
[9] M. López-López, C. García-Ruiz, *Trends Anal. Chem.* **2014**, *54*, 36.
[10] H. Cui, S. Li, S. Deng, H. Chen, C. Wang, *ACS Sens.* **2017**, *2*, 386.
[11] L. Qu, N. Wang, H. Xu, W. Wang, Y. Liu, L. Kuo, T. P. Yadav, J. Wu, J. Joyner, Y. Song, H. Li, J. Lou, R. Vajtai, P. M. Ajayan, *Adv. Funct. Mater.* **2017**, *27*, 1701714.
[12] S.-G. Park, C. Mun, X. Xiao, A. Braun, S. Kim, V. Giannini, S. A. Maier, D.-H. Kim, *Adv. Funct. Mater.* **2017**, *27*, 1703376.
[13] C. Song, L. Min, N. Zhou, Y. Yang, S. Su, W. Huang, L. Wang, *ACS Appl. Mater. Interfaces* **2014**, *6*, 21842.
[14] Y. H. Lee, W. Shi, H. K. Lee, R. Jiang, I. Y. Phang, Y. Cui, L. Isa, Y. Yang, J. Wang, S. Li, *Nat. Commun.* **2015**, *6*, 6990.
[15] C. Tian, C. Ding, S. Liu, S. Yang, X. Song, B. Ding, Z. Li, J. Fang, *ACS Nano* **2011**, *5*, 9442.
[16] J. Fang, S. Du, S. Lebedkin, Z. Li, R. Kruk, M. Kappes, H. Hahn, *Nano Lett.* **2010**, *10*, 5006.
[17] Z. Liu, Z. Yang, B. Peng, C. Cao, C. Zhang, H. You, Q. Xiong, Z. Li, J. Fang, *Adv. Mater.* **2014**, *26*, 2431.
[18] A. Garcia-Leis, J. V. Garcia-Ramos, S. Sanchez-Cortes, *J. Phys. Chem. C* **2013**, *117*, 7791.
[19] M. S. Strozyk, D. J. de Aberasturi, J. V. Gregory, M. Brust, J. Lahann, L. M. Liz-Marzán, *Adv. Funct. Mater.* **2017**, *27*, 1701626.
[20] D. Jimenez de Aberasturi, A. B. Serrano-Montes, J. Langer, M. Henriksen-Lacey, W. J. Parak, L. M. Liz-Marzán, *Chem. Mater.* **2016**, *28*, 6779.
[21] M. L. Tseng, Y.-W. Huang, M.-K. Hsiao, H. W. Huang, H. M. Chen, Y. L. Chen, C. H. Chu, N.-N. Chu, Y. J. He, C. M. Chang, *ACS Nano* **2012**, *6*, 5190.
[22] K. Xu, C. Zhang, R. Zhou, R. Ji, M. Hong, *Opt. Express* **2016**, *24*, 10352.
[23] H. B. Jiang, Y. L. Zhang, D. D. Han, H. Xia, J. Feng, Q. D. Chen, Z. R. Hong, H. B. Sun, *Adv. Funct. Mater.* **2014**, *24*, 4595.
[24] C. Zhang, K. Lin, Y. Huang, J. Zhang, *Sensors* **2017**, *17*, 1462.
[25] P. C. Wuytens, A. G. Skirtach, R. Baets, *Opt. Express* **2017**, *25*, 12926.
[26] P. C. Wuytens, A. Z. Subramanian, W. H. De Vos, A. G. Skirtach, R. Baets, *Analyst* **2015**, *140*, 8080.
[27] L. Liu, H. Yang, X. Ren, J. Tang, Y. Li, X. Zhang, Z. Cheng, *Nanoscale* **2015**, *7*, 5147.
[28] G. Sinha, L. E. Depero, I. Alessandri, *ACS Appl. Mater. Interfaces* **2011**, *3*, 2557.
[29] X. Li, H. Hu, D. Li, Z. Shen, Q. Xiong, S. Li, H. J. Fan, *ACS Appl. Mater. Interfaces* **2012**, *4*, 2180.
[30] Y. Zhao, L. Sun, M. Xi, Q. Feng, C. Jiang, H. Fong, *ACS Appl. Mater. Interfaces* **2014**, *6*, 5759.
[31] X. Zou, R. Silva, X. Huang, J. F. Al-Sharab, T. Asefa, *Chem. Commun.* **2013**, *49*, 382.
[32] X. He, H. Wang, Q. Zhang, Z. Li, X. Wang, *Eur. J. Inorg. Chem.* **2014**, *2014*, 2432.
[33] Y. Zang, J. Yin, X. He, C. Yue, Z. Wu, J. Li, J. Kang, *J. Mater. Chem. A* **2014**, *2*, 7747.
[34] X. Zhang, Y. Zhu, X. Yang, Y. Zhou, Y. Yao, C. Li, *Nanoscale* **2014**, *6*, 5971.

[35] H. Dai, Y. Sun, P. Ni, W. Lu, S. Jiang, Y. Wang, Z. Li, Z. Li, *Sens. Actuators B* **2017**, *242*, 260.
[36] X. Li, G. Chen, L. Yang, Z. Jin, J. Liu, *Adv. Funct. Mater.* **2010**, *20*, 2815.
[37] K. Xu, J. Wu, C. F. Tan, G. W. W. Ho, A. Wei, M. Hong, *Nanoscale* **2017**, *9*, 11574.
[38] S.-H. Li, S. Liu, J. C. Colmenares, Y.-J. Xu, *Green Chem.* **2016**, *18*, 594.
[39] S. Liu, M.-Q. Yang, Z.-R. Tang, Y.-J. Xu, *Nanoscale* **2014**, *6*, 7193.
[40] G. Wang, K. Li, F. J. Purcell, D. Zhao, W. Zhang, Z. He, S. Tan, Z. Tang, H. Wang, E. Reichmanis, *ACS Appl. Mater. Interfaces* **2016**, *8*, 24974.
[41] X. Pan, M.-Q. Yang, X. Fu, N. Zhang, Y.-J. Xu, *Nanoscale* **2013**, *5*, 3601.
[42] J. Huang, D. Ma, F. Chen, D. Chen, M. Bai, K. Xu, Y. Zhao, *ACS Appl. Mater. Interfaces* **2017**, *9*, 7436.
[43] H. Li, Z. Su, S. Hu, Y. Yan, *Appl. Catal. B* **2017**, *207*, 134.
[44] Q. Zhang, J. Wang, D. Xu, Z. Wang, X. Li, K. Zhang, *J. Mater. Chem. A* **2014**, *2*, 3865.
[45] Q. Zhang, K. Zhang, D. Xu, G. Yang, H. Huang, F. Nie, C. Liu, S. Yang, *Prog. Mater. Sci.* **2014**, *60*, 208.
[46] X. Liu, Z. Li, Q. Zhang, F. Li, T. Kong, *Mater. Lett.* **2012**, *80*, 37.
[47] N. D. Hoa, N. Van Quy, H. Jung, D. Kim, H. Kim, S.-K. Hong, *Sens. Actuators B* **2010**, *146*, 266.
[48] X. Wang, X. Wu, L. Yuan, K. Huang, S. Feng, *Mater. Des.* **2017**, *113*, 297.
[49] Z. Fan, X. Fan, A. Li, L. Dong, *Nanoscale* **2013**, *5*, 12310.
[50] M. Chen, Y. Yue, Y. Ju, *J. Appl. Phys.* **2012**, *111*, 104305.
[51] D. Malwal, P. Gopinath, *Catal. Sci. Technol.* **2016**, *6*, 4458.
[52] L. Ma, H. Wu, Y. Huang, S. Zou, J. Li, Z. Zhang, *ACS Appl. Mater. Interfaces* **2016**, *8*, 27162.
[53] Y. Lin, C. E. Bunker, K. A. Fernando, J. W. Connell, *ACS Appl. Mater. Interfaces* **2012**, *4*, 1110.
[54] J. Bian, S. Shu, J. Li, C. Huang, Y. Y. Li, R.-Q. Zhang, *Appl. Surf. Sci.* **2015**, *333*, 126.
[55] C. Jean, L. Belliard, T. W. Cornelius, O. Thomas, Y. Pennec, M. Cassinelli, M. E. Toimil-Molares, B. Perrin, *Nano Lett.* **2016**, *16*, 6592.
[56] C.-L. Hsu, J.-Y. Tsai, T.-J. Hsueh, *Sens. Actuators B* **2016**, *224*, 95.
[57] L.-L. Lu, J. Ge, J.-N. Yang, S.-M. Chen, H.-B. Yao, F. Zhou, S.-H. Yu, *Nano Lett.* **2016**, *16*, 4431.
[58] X.-Q. Wang, C. F. Tan, K. H. Chan, K. Xu, M. Hong, S.-W. Kim, G. W. Ho, *ACS Nano* **2017**, *11*, 10568.
[59] K. Xu, C. Zhang, T. H. Lu, P. Wang, R. Zhou, R. Ji, M. Hong, *Opto-Electron. Eng.* **2017**, *44*, 185.